

# A variable star population in the open cluster NGC 6791 observed by the *Kepler* spacecraft

S. Sanjayan<sup>1,2</sup>, A.S. Baran<sup>1,3,4</sup>, P. Németh<sup>1,5,6</sup>, K. Kinemuchi<sup>7,8</sup>, J. Ostrowski<sup>1</sup> and S.K. Sahoo<sup>1,2</sup>

<sup>1</sup>ARDA STELLA Research Group, Institute of Physics, Pedagogical University of Cracow,  
ul. Podchorążych 2, 30-084 Kraków, Poland

<sup>2</sup>Centrum Astronomiczne im. Mikołaja Kopernika, Polskiej Akademii Nauk, ul. Bartycka 18, 00-716 Warszawa, Polska

<sup>3</sup>Embry-Riddle Aeronautical University, Department of Physical Sciences, Daytona Beach, FL 32114, USA

<sup>4</sup>Department of Physics, Astronomy, and Materials Science, Missouri State University, Springfield, MO 65897, USA

<sup>5</sup>Astroserver.org, Fő tér 1, 8533 Malomsok, Hungary

<sup>6</sup>Astronomical Institute of the Czech Academy of Sciences, Fričova 298, CZ-251 65 Ondřejov, Czech Republic

<sup>7</sup>Department of Astronomy, New Mexico State University, Box 30001, MSC 4500, Las Cruces, NM 88003, USA

<sup>8</sup>Apache Point Observatory, 2001 Apache Point Road, P.O. Box 59, Sunspot, NM 88349-0059

April 15, 2022

## Abstract

We present the list of variable stars we found in the *Kepler* superstamp data covering approximately 9 arcminutes from the central region of NGC 6791. We classified the variable stars based on the variability type and we established their cluster membership based on the available *Gaia* Early Data Release 3 astrometry, by means of the Bayesian Gaussian mixture models. In total we found 278 variable objects, among which 17 binaries, 45 pulsators, 62 rotational and five unclassified variables are cluster members. The remaining 28 binaries, 25 pulsators, 83 rotational, four unclassified and nine unidentified variables are either not members or their membership is not established. In the case of eclipsing binaries we calculated the mid-times of eclipses and derived ephemerides. We searched for eclipse timing variation by means of the observed minus calculated diagrams. Only three objects show significant orbital period variation. Independently of a report published just recently by Colman *et al.* (2022) we found 119 new variables. We used isochrones calculated within the MIST project and derived the age (8.91 Gyr), average distance (4134 pc) and iron content [Fe/H] (0.26-0.28), of NGC 6791. Using the cluster members with membership probabilities greater than 0.9, we calculated the distance to the cluster of 4123(31) pc, which agrees with the result from our isochrone fitting.

**Open clusters and associations : individual: NGC 6791 – binaries: general – Stars oscillations – Stars : rotation**

# 1. Introduction

NGC 6791 has been first described as a metal rich cluster by Baade (1931) and listed as an old open cluster by King (1964). The authors provided no age estimations. Kinman (1965) presented a detailed comparative study of color – magnitude diagrams (CMD) of NGC 6791 along with other two open clusters, M 67 (4 Gyr) and NGC 188 (6.8 Gyr). From the first photometric observations in the B-V color, Harris and Canterna (1981) determined a reddening of  $E(B-V) = 0.13$  mag. According to the recent studies NGC 6791 is 7–9 Gyr old (Chaboyer *et al.* 1999, Carraro *et al.* 2006, Basu *et al.* 2011), and it has a mass of around  $4000 M_{\odot}$  (Kaluzny and Udalski 1992, Carraro *et al.* 2006, Platais *et al.* 2011, Tofflemire *et al.* 2014). The cluster is located  $\sim 8000$  pc from the Galactic center and 1000 pc above the Galactic plane. According to some hypotheses the cluster may have formed in the bulge of the Galaxy and radially migrated to its current location (Jilkova *et al.* 2012, Villanova *et al.* 2018). The distance to the cluster is approximately 3614 pc, which was estimated for the first time by Stetson *et al.* (2003) from the de-reddened distance modulus of  $(m-M)_0 \approx 12.79$  mag. The authors derived  $E(B-V) = 0.09$  mag. According to Villanova *et al.* (2018) NGC 6791 is a super metal-rich cluster with  $[Fe/H] = +0.3 - +0.4$ . Geisler *et al.* (2012) showed that NGC 6791 has multiple stellar populations, which makes the cluster chemically peculiar. NGC 6791 has an anomalous horizontal branch with a red clump (RC) region. Liebert *et al.* (1994) found a group of extreme horizontal branch members using spectrophotometry of blue targets observed by Kaluzny and Udalski (1992). The age of the cluster predicts that it should have a rich population of cooling white dwarfs, hence Bedin *et al.* (2005) observed the cluster using the Hubble Space Telescope up to  $m_{F606W} \approx 28.5$  mag. They found the white dwarf luminosity function to give a peak at 27.4 mag, which corresponds to an age of 2.5 Gyr. Such an estimate does not agree with the age derived from the main sequence (MS) or red giant branch (RGB) population (Chaboyer *et al.* 1999, Carraro *et al.* 2006). Thus far, these studies show the cluster is very unusual. A more detailed study is required to constrain the age and metal abundances for understanding the formation and evolution of NGC 6791. A clear picture of the cluster could be achieved by deriving an entire population of variable stars and analysis of components of the stars to find their ages and chemical abundances.

NGC 6791 has been a subject of extensive search for variable stars. Kaluzny and Udalski (1992) and Kaluzny and Rucinski (1993) did an extensive photometric survey finding 17 variable stars which includes 8 contact binaries, two blue stragglers and one binary consisting of a hot subdwarf B star. Rucinski *et al.* (1996) found three detached binaries and one cataclysmic variable (CV) star exhibiting a three day outburst. As a part of search for planets in stellar clusters, Mochejska *et al.* (2002) found 47 new low amplitude variable stars. The authors reported several BY Dra type and two outbursting CV stars, confirming the CV found by Rucinski *et al.* (1996). Mochejska *et al.* (2003) reported seven new variable stars with a long and periodic flux variation. Kaluzny (2003) found four new variable stars by reanalyzing archived data from Kaluzny and Rucinski (1993). A search for transiting events by giant planets reported by Bruntt *et al.* (2003) yielded 22 new low amplitude objects along with 20 previously known variable stars. Using a

high precision time-series photometry, Hartman *et al.* (2005) detected 10 new variable stars including one  $\delta$ -Scuti type star and 8 contact binaries. Mochejska *et al.* (2005) detected 14 more variable stars and reported 9 eclipsing binaries. Using a high precision photometry in the Johnson V band, de Marchi *et al.* (2007) detected 260 variables in the cluster area, although not all stars are members of the cluster.

From the launch in 2009, for almost 10 years the *Kepler* spacecraft has served mankind by providing very precise and almost continuous photometric measurements (Koch *et al.* 2010). The *Kepler* has observed more than five hundred thousand stars during its entire mission time. The *Kepler* mission was completed in two phases. During the first mission, *Kepler* observed 0.25% of the sky in the direction of Cygnus and Lyra constellation for 1460 days. The mission was reborn as K2 (second mission) after the second reaction wheel failed. K2 mission made 80 day observing campaigns along the ecliptic equator, which lasted 1695 days (Howell *et al.* 2014). During both missions, the observations were obtained using two different exposures, 30 minutes for the long cadence (LC) and 1 minute for the short cadence (SC) mode (Koch *et al.* 2010, Borucki *et al.* 2010, Caldwell *et al.* 2010, Thompson *et al.* 2016). During the first mission, four open clusters were inside the *Kepler* field of view, NGC 6791, NGC 6819, NGC 6811 and NGC 6866. Two of the open clusters, NGC 6791 and NGC 6819, were observed by using the so-called LC superstamps.

Recently, Colman *et al.* (2022) presented light curves of KIC stars obtained from the *Kepler* superstamp data. The authors used an image subtraction method to derive light curves of all *Kepler* cataloged targets. They identified variability in 239 out of 5342 stars they extracted light curves of. The number of new variables is not given. We stress that our work has been performed simultaneously to, yet independently from, Colman *et al.* (2022) and contains additional analysis. By comparing our results with results of Colman *et al.* (2022), we have noticed that the authors applied a very strong detrending policy removing either eclipses or out-of-eclipse variations in binaries or variations in other objects that we claim to be variables.

In Section 2 of this paper, we present a brief description of the *Kepler* data and method used for obtaining the light curves of variable objects. In Section 3, we present a spectroscopic study of the variable stars found in this project using either archived spectra from public surveys or our own data. In Section 4, we describe the method of deriving the membership probabilities of our new variable star findings. In Section 5, we report individual variable star cluster members divided into variability classes. The field variable counterparts are listed in the Tables 5–8. In Section 6, we present the result of isochrone fitting.

## 2. Kepler Photometry

We downloaded the *Kepler* superstamp data of NGC 6791 from the Mikulski Archive for Space Telescopes (MAST<sup>1</sup>). The data are 20 x 100 pixel boxes piled up in two contiguous 10 box stacks. The field of view of all pixels is

---

<sup>1</sup><https://archive.stsci.edu/>

800 x 800 arcseconds and covers the most central part of the cluster. The superstamps data are collected in the LC mode. The pixel scale of an individual square pixel is 4 arcsec. The data have been collected over 1460 days and are split into 18 quarters.

We searched for a flux variation by extracting fluxes for all time stamps in individual pixels for each of the quarters Q2–5. Then, a Fourier transform of the time-series data was performed in each pixel and each quarter separately. The pixels showing peaks (representing signal) in the amplitude spectra were selected. Signals that were identified with artifacts, either reported by Baran (2013) or those found in this project, were discarded. We combined all contiguous pixels showing the same signal and defined an optimal aperture of pixels. To keep the solar cells exposed to the sunlight, every quarter the spacecraft rolled 90 degrees, hence, with each quarterly rotation of the spacecraft, our targets landed on different CCD chips. This positioning caused different target images, and consequently, different optimal apertures (Bryson *et al.* 2010). Fortunately, every four quarters the images and apertures were the same, so we have defined the apertures only in four quarters, i.e. Q2–5, and propagate them to the corresponding quarters (e.g. Q2, 6, 10, 14). Next, using the optimal apertures for all targets showing flux variation we used PyKE software (Kinemuchi *et al.* 2012) to pull out the fluxes and correct them for instrumental artifacts by means of Co-trending Basis Vectors. Finally, using our custom scripts, we clipped the data at 4.5 sigma, detrended using spline fits, and normalized them to *parts per thousand* (ppt). The variable stars discovered in our work will be presented in Section 5.

### 3. Spectroscopy

We searched for spectra in the literature of all variables we detected. We found optical or infrared spectra for 111 objects in the archives of APOGEE (Ahn *et al.* 2014, Majewski *et al.* 2017), SDSS (Blanton *et al.* 2017), LAMOST (Zhao *et al.* 2012), ESO (Gilmore *et al.* 2012, Randich *et al.* 2013), and the HECTOSPEC (Fabricant *et al.* 2005) surveys. All spectra with  $T_{\text{eff}} < 15\,000\text{ K}$  were modeled with interpolated local thermal equilibrium (LTE) synthetic spectra drawn from the BOSZ (Bohlin *et al.* 2017) spectral library to determine the fundamental atmospheric parameters. The BOSZ library was calculated for scaled solar metallicity with carbon and  $\alpha$ -element enhancement; therefore, individual abundance patterns cannot be investigated with our method.

Our fitting procedure (XTGRID; Németh *et al.* 2012) is based on a steepest-gradient chi-square minimizing method, which was originally developed to model hot stars. To improve its performance for cool stars, we added a grid-search preconditioning to the procedure. We step through a set of models to search for the best starting model for the steepest-descent part. Next, the descent part takes over in driving the fit and converges on the best solution. Once a convergence is achieved, the procedure explores the parameter errors by stepping through a set of points around the best solution. If a better solution is found during error calculations, then the procedure returns to the descent part, and hence pushing the solution towards the global minimum. XTGRID fits the radial velocity and projected rotation velocity of each

spectra along with the stellar surface parameters, such as the effective temperature ( $T_{\text{eff}}$ ), surface gravity ( $\log g$ ) and abundances.

In addition, the procedure accesses photometric data from the VizieR Photometry Viewer<sup>2</sup>, distance data from the Gaia EDR3 database, and extinction values from the NED online services. The spectroscopic surface parameters combined with these measurements allow us to reduce systematics and derive absolute stellar parameters, such as mass, radius, and luminosity. An anti-correlation is observed between  $T_{\text{eff}}$  and  $[\text{Fe}/\text{H}]$ . Fortunately, the spectral energy distribution (SED) helps in resolving this bias by restricting the  $T_{\text{eff}}$ . Another bias is observed in surface gravity, in particular below  $T_{\text{eff}} = 4\,000$  K. At such low temperatures, the spectrum is insensitive to the surface gravity. When the spectral coverage is very limited, we could not determine an accurate value for  $\log g$ . We do not report atmospheric parameters for such stars.

The archival spectroscopic data are very inhomogeneous. Consequently, high resolution spectra (e.g. obtained with ESO instruments) with a short wavelength coverage are more suitable for radial velocity measurements, while low resolution spectra (e.g. from the SDSS and LAMOST surveys) can provide more consistent atmospheric parameters, but less precise velocities. Some ESO spectra cover only 5 300-5 600 Å range at a resolution of  $R=20\,000$ , and only weak spectral features are visible. For such spectra, at a relatively low signal-to-noise ratio (SNR), the fitting procedure increases the projected rotation above  $100\text{ km s}^{-1}$ , which decreases the radial velocity accuracy. In general, low SNR spectra limit our analysis the most, while crowding in dense stellar fields and a limited spectral coverage affects the parameter determination.

## 4. Cluster membership

We used *Gaia* astrometry to determine the membership probabilities of all variable stars we found. We used five parameters, i.e. equatorial coordinates  $\alpha$  and  $\delta$ , proper motions  $\mu_\alpha$  and  $\mu_\delta$ , and parallax  $\pi$  (further called five astrometric parameters). First, we adopted/estimated mean values of these parameters. The cluster center has been taken from Kamann *et al.* (2019) to be at  $\alpha_{2000} = 19:20:51.3$  and  $\delta_{2000} = +37:46:26$ . Next, we downloaded *Gaia* Early Data Release 3 (EDR3) (*Gaia* collaboration *et al.* 2016, 2021) data for all stars within a tidal radius of 23 arcmin (Platais *et al.* 2011). The area contains 36 647 targets accessible to our analysis; however, we filtered out dubious targets with parallaxes to be negative or greater than 1 arcsec or relative uncertainties for any of the proper motion or parallax values to be greater than 50%. A cluster environment, particularly toward the center, is very dense, which can lead to unrealistic or imprecise estimates of these three parameters ( $\mu_\alpha$ ,  $\mu_\delta$ ,  $\pi$ ). In addition, we limited our sample to targets for which the zero point offset corrections of parallax have been applied (Lindegren *et al.* 2021). After filtering and correcting for the parallax zero offset, we ended up with 11 466 targets.

<sup>2</sup><http://vizier.u-strasbg.fr/vizier/sed/>

To determine the membership probabilities, we used the Bayesian Gaussian Mixture Models (GMM) using *scikit-learn* python toolkit (Pedregosa *et al.* 2011). The GMM assumes each data point to be a combination of finite Gaussian functions, in which the number of these functions is determined using a variational Bayesian inference model with Dirichlet process prior (Ferguson 1973). We performed 10 000 iterations using the Expectation–Maximization algorithm (Dempster *et al.* 1977), and we derived membership probabilities for each target in our sample based on all five astrometric parameters. In the case of targets that we found variables in the superstamp area, we estimated their membership probabilities regardless of precision of their five astrometric parameters. If the uncertainties were larger than 50%, we considered corresponding parameters to be error-free, while the negative parallaxes were ignored and only four astrometric parameters were used.

To strengthen the probability, the radial velocity of individual stars can also be used, however they need to be corrected for the effects of binarity, rotation, and pulsations. Different instruments differ in instrumental calibration which often bias the radial velocity (RV) estimates. Since we did not conduct one single survey that could provide us with consistent RV estimations, we decided not to use RVs for the membership analysis. Since binarity and rotation affects the measurement of intrinsic motion, we expect the RVs will be random values and, as it will be seen in Section 5, the values in Tables 1–3, confirm our suspicion. We expected the most consistent estimates for single solar-like pulsators, since their oscillation motion on the surface is of a very small amplitude. In fact, in only three cases the RVs are far from the average cluster value ( $-47.46 \pm 1.08$  km/s, Carrera *et al.* 2019), since the stars may belong to binary systems. On the other hand, RVs that are consistent indicate that the stars are likely single or the orbital motion (if any) is very slow or the spectra have been taken when both stars were aligned with the observer’s line of sight. The RVs of the solar-like stars that are unlikely to be members (Table 6) are not close to the cluster average and seem to confirm their field membership, unless they are in binaries.

## 5. A zoo of variable stars

In total, we found 278 variable objects in the superstamp area. Our sample contains cluster members as well as foreground and background stars. In Section 4, we provided details on a membership analysis. Our prime focus is on the members of NGC 6791. The non-members and objects with unknown membership status, as a consequence of a lack of the *Gaia* astrometry, are listed in the Table 5-8. Their variability is classified the same way as for the cluster members.

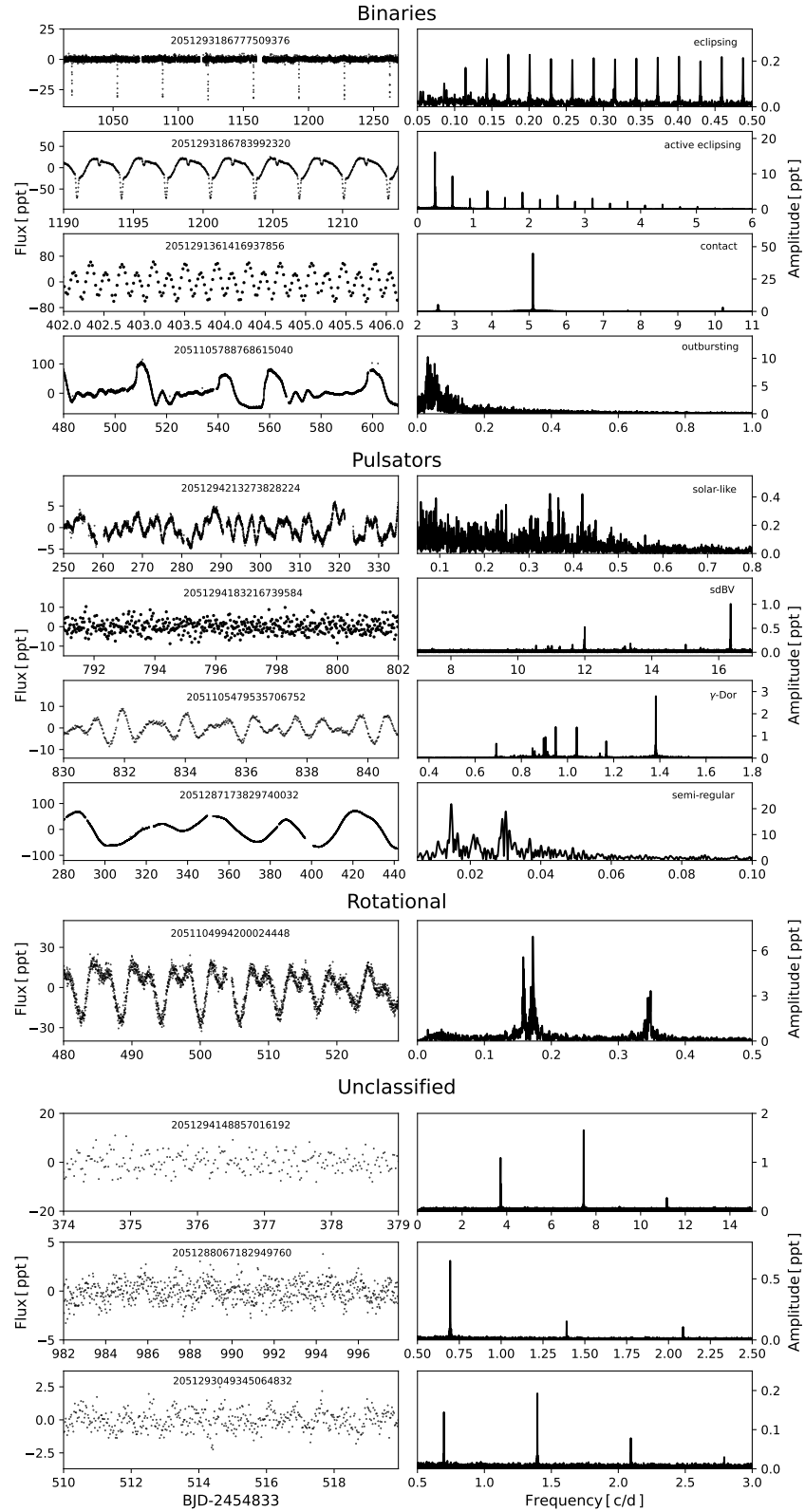


Figure 1: Examples of light curves and corresponding amplitude spectra of a zoo of variable stars in the open cluster NGC 6791.

Based on flux variations, we classified the stars into three main variability types, i.e. eclipsing, pulsating, and rotating stars. The first two types are further split into specific classes. Five stars remained unclassified. Their light curves show variations that we are unable to unambiguously identify as one of the three types listed. These objects show flux variations which can origin in *e.g.* a reflection effect, ellipsoidal variation or a rotation of a spotted star. These stars have typically low amplitude flux variations. In Fig. 1 we present examples of light curves and their corresponding amplitude spectra for each type and a selection of classes of variable stars we found.

## 5.1 Binary systems

We selected binary stars with sharp eclipses typical for semi- and detached systems. Some eclipsing systems show additional out-of-eclipse variation, which can be caused by a chromospheric activity, and we call them "active" eclipsing. We identified contact systems, which are characterized by a continuous flux change and typical for W UMa stars. Another class contains outbursting stars, which we associate with binaries experiencing a rapid mass transfer causing sudden eruptions, *e.g.* novae, dwarf novae, nova-like variables. We stress that our classification is not based on radial velocities. Some of the stars may not be classified correctly, *e.g.* a smoothly continuous and small amplitude flux changes may be misidentified with rotational variables. However, the flux change over the course of observations is not modulated (see explanation in Section 5.3) or they can be long-period pulsating stars. In Fig. 2 we present the phased light curves of three stars that we consider new discoveries. The sample includes all the classes of binary stars we identified in the superstamp data. We found 17 binaries to be cluster members (Table 1), 28 binaries are field objects, including two binaries for which we could not establish membership due to the lack of *Gaia* astrometry data (Table 5). For binary systems their membership has been derived based on all five astrometric parameters. Majority of binaries in the cluster are main sequence (MS) stars with just two exceptions, assuming the position of the latter in the CMD is correct. *Gaia* EDR3 2051105720053889536 is a post-MS star on its early ascent of the red giant branch (RGB), while *Gaia* EDR3 2051293186783992320 is located below the RGB, which can be explained by an incorrect color index or pre-MS evolutionary status. Among the member counterparts, five are eclipsing, six active eclipsing, five contact, and one outbursting stars.



Table 1: List of binary stars that are cluster members.

<i>Gaia</i> EDR3	KIC	$P_{\text{orb}}$ [days]	$T_0$ [BJD]	G	CMD	HRD	$T_{\text{eff}}$ [K]	logg	RV [km/s]	[Fe/H]	Ref
2051287203888386688	2436378 <sup>10L</sup>	8.531633(8)	2 454 969.2757(8)	eclipsing	MS <sup>+</sup>	—	—	—	—	—	—
<b>2051288372129693440</b>	2569175 <sup>X</sup>	43.499395(21)	2 455 041.61331(38)	18.383	MS	RGB	5 620(40)	3.517(18)	-65.8(4)	-0.67(9)	2*
2051292980625561216	2437149 <sup>2S,6L</sup>	18.7986285(37)	2 454 971.02807(16)	17.480	MS	MS+MS	5 100(900)	4.5(4)	-80.9(9)	-0.25(25)	2*
<b>2051293083698347008</b>	2437482 <sup>X</sup>	17.551175(14)	2 454 966.9452(7)	18.210	MS	RGB	4 860(50)	3.042(20)	-67.5(5)	-0.48(15)	1*
<b>2051293186777509376</b>	2437041 <sup>X</sup>	34.859569(14)	2 454 979.90568(33)	18.055	MS	MS	6 360(40)	4.58(7)	-57.0(8)	-0.42(11)	2*
2051105342091761536	2437783 <sup>4L</sup>	7.453112(10)	2 454 964.7652(11)	18.391	MS	BS	7 160(50)	3.60(8)	-20.1(6)	-0.82(9)	2*
205110554825223680	2438490 <sup>4L</sup>	3.3157657(10)	2 454 967.85556(27)	17.887	MS <sup>+</sup>	HB	5 410(90)	2.87(7)	-62.2(12)	-0.68(15)	2*
2051105784476572032	2438061 <sup>1S,12L</sup>	4.8858826(16)	2 454 965.01144(28)	17.721	MS	HB	5 220(30)	2.197(10)	-46.5(45)	0.42(22)	1*
2051293186783992320	2437060 <sup>6L</sup>	3.1871038(8)	2 454 969.04204(21)	16.989	RGB	MS	5 270(20)	4.253(45)	-59.6(7)	-0.445(47)	1*
2051294423734919552	2569494 <sup>1S,5L</sup>	1.5232747(12)	2 454 965.3339(7)	17.288	MS	MS	5 580(50)	4.06(6)	-116(8)	-0.36(11)	1*
2051295351447975168	2570480 <sup>X</sup>	0.7349394(16)	2 454 964.9628(18)	19.340	MS <sup>+</sup>	HB	5 870(160)	2.34(11)	41.2(30)	-0.14(7)	2*
2051105543955885696	2438413 <sup>X</sup>	0.31754621(10)	2 454 964.63952(27)	18.281	MS	RGB	5 380(100)	3.347(38)	-34.70(13)	-0.631(46)	2*
2051105720053889536	2438148 <sup>X</sup>	0.29468323(11)	2 454 964.79285(30)	16.612	RGB	—	—	—	—	—	—
2051291361416937856	2568950 <sup>X</sup>	0.3917614(15)	2 454 964.91341(33)	17.555	MS	MS/RGB	5 300(20)	3.926(20)	-39.50(10)	-1.131(26)	1*
2051293324222974976	2569965 <sup>X</sup>	0.325587259(49)	2 454 964.71162(13)	17.510	MS <sup>+</sup>	MS	5 380(20)	4.46(8)	-63(6)	-0.36(8)	1*
2051294114497255936	2569630 <sup>X</sup>	0.31265938(26)	2 454 964.7815(7)	16.964	MS	MS	5 620(50)	4.030(56)	-41(2)	-0.14(9)	1*
2051105788768615040	2438114 <sup>4L</sup>	32.27	—	18.192	blue of MS <sup>+</sup>	blue of MS	27 000(5 000)	7.3(6)	-34(25)	-1(1)	1*

The stars that we consider newly detected variables are marked in **bold**. The superscripts in the KIC column denote if the data are available on the MAST: X stands for no data, L and S stand for the LC and SC data, respectively, and the numbers represent a total number of quarters the data were taken in. CMD refers to a position in the color-magnitude diagram (MS - main sequence, RGB - red giant branch, BS - blue straggler, AGB - asymptotic giant branch, RC - red clump, HB - horizontal branch, EHB - extreme horizontal branch). HRD refers to a position in the  $T_{\text{eff}}$ , log  $g$  diagram. The <sup>+</sup> symbol indicates that *not* all five astrometric parameters were used in the membership analysis. The Ref column refers to the source of the spectra, i.e. 1 - HECTOSPEC, 2 - ESO, 3 - LAMOST, 4 - SDSS and 5 - APOGEE. The \* indicates that the atmospheric parameters are derived in this work. HECTOSPEC - <https://oirsa.cfa.harvard.edu>, ESO - <http://archive.eso.org>, APOGEE - <https://www.sdss.org/dr16/irspec>, LAMOST - <http://dr6.lamost.org>, SDSS - <http://skyserver.sdss.org/dr16>

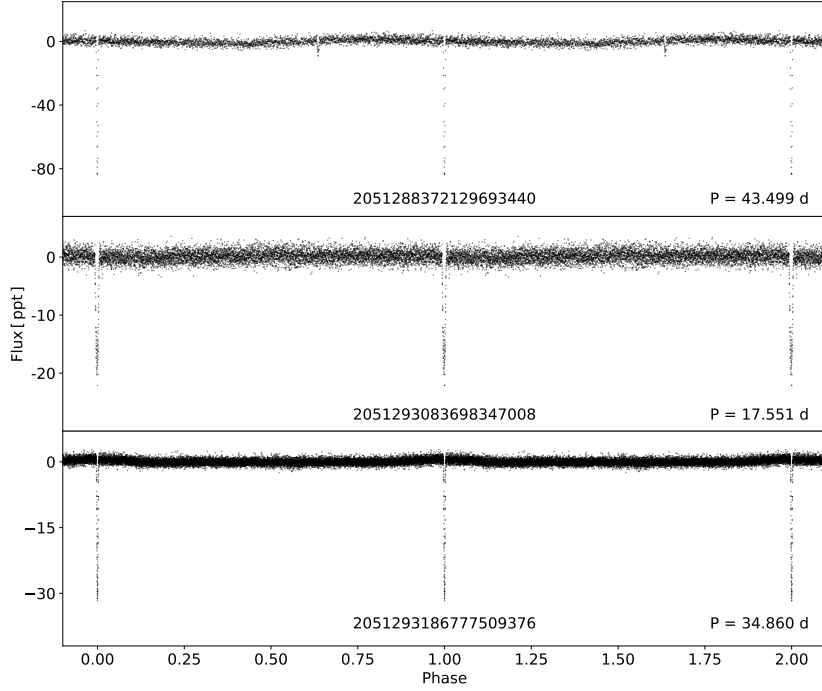


Figure 2: Phased light curves of three newly discovered binary star members of NGC 6791.

Since the objects considered in this section are binaries, magnitudes and color indices used in the top panel of Fig. 3 and  $T_{\text{eff}}$  and  $\log g$  in the top panel of Fig. 6 (this figure will be explained in Section 6) may be averages of all components in a specific binary system and may not indicate a proper location of individual stars in the CMD. If the average location in the CMD diagram is in the well defined regions, e.g. MS or RGB, we can expect the components are of similar properties (or a secondary component is not detectable in our data), and the average is not far from single star values (unless the binary components are much different but the shift is only along a given evolutionary stage, e.g. along the RGB branch). If the location is outside those regions, e.g. below MS or RGB, then the individual components in a binary system are not alike, e.g. WD + MS, and the average will be somewhere between a WD track and the MS (as is the case for *Gaia* EDR3 2051105788768615040). For this same reason, the RV of binaries is typically different from the average RV of a cluster. We expect the orbital RV to be dominating. There are only one exception with the RV being close to the average cluster value. In the case of *Gaia* EDR3 2051105784476572032 the spectrum could have been taken during the eclipse or it is a spectroscopic single-line binary.

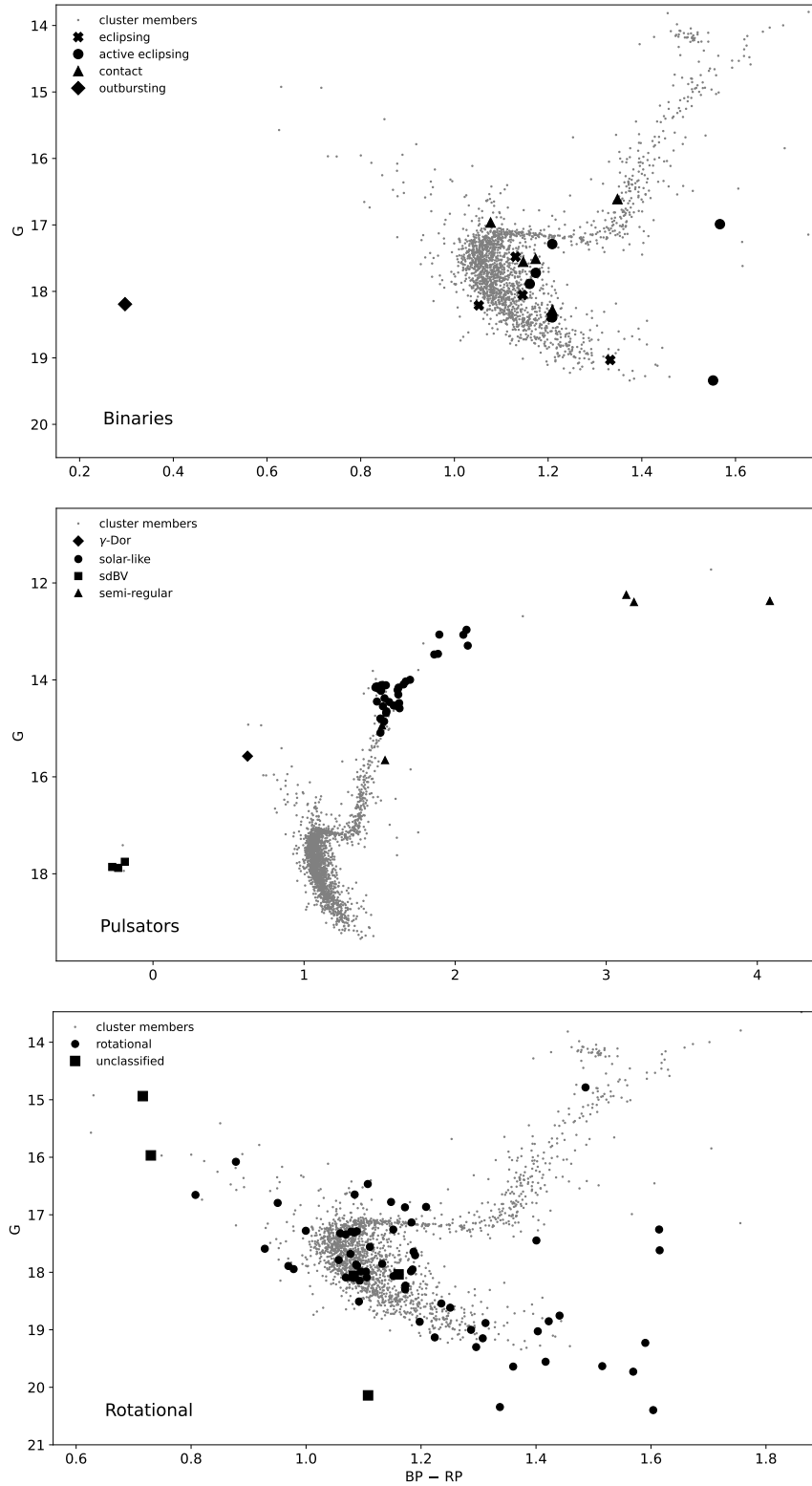


Figure 3: The color-magnitude diagram for NGC 6791. We listed variable stars such as binaries, pulsators and rotational cluster members in the top, middle and bottom panels, respectively. Unclassified stars are plotted in the bottom panel.

We estimated the mid-times of eclipses or, in the case of non-eclipsing systems, a minimum of a light variation by means of the method described in Kwee & van Woerden (1956). We used the mid-times to derive the ephemeris, i.e. a reference epoch, defined as the first mid-time in a given dataset, and an orbital period for each binary system we found. We provided estimates of these two parameters in Table 1 and Table 5. The exceptions are systems for which the data are very noisy, not allowing us to derive precise mid-times, and outbursting stars. For these systems we reported only rough estimates (arbitrarily adopted two decimal places for precision) of their orbital periods, derived from the Fourier amplitude spectra. The ephemerides were used to calculate the Observed - Calculated (O-C) diagrams to check on the orbital period variation. For most of the stars the O-C diagrams do not show any significant period variation. The exceptions are shown in Fig. 4. *Gaia* EDR3 2051294114497255936 (the top panel of Fig. 4) shows quite a large amplitude period variation with only one full cycle covered. These two O-C diagrams are constructed based on an average primary and secondary eclipses. *Gaia* EDR3 2051105342091761536 (the bottom panel of Fig. 4) shows cyclic variations of the orbital period derived solely from primary eclipses. To explain a periodic change an additional body in the system can be invoked. To test this hypothesis and, if confirmed, to constrain the parameters of those bodies, RV time-series data are required.

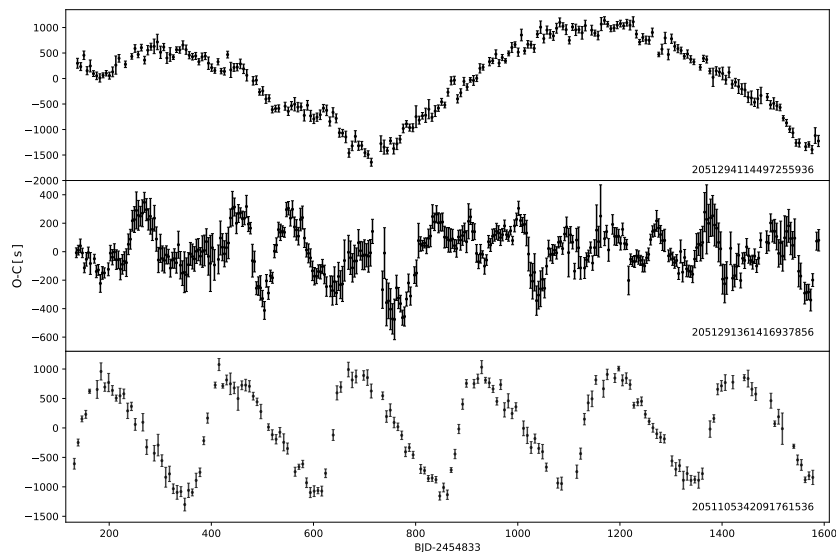


Figure 4: O-C diagrams for three binary systems that show variation of the orbital period.

## 5.2 Pulsators

We found 70 objects that show an intrinsic variability caused by stellar oscillations. We identified the following types of pulsators, i.e.  $\delta$  Scuti and  $\gamma$ -Dor, solar-like along the RGB, RR Lyr, pulsating hot subdwarf B stars (sdBV) on the EHB, and semi-regular along the RGB and AGB. In Table 2 we show only the cluster member counterpart, while the

field pulsators are listed in Table 6.

Among the cluster members we found one blue straggler, 36 solar-like pulsators (10 being RC objects, while 26 are still on the RGB), three sdBVs and five semi-regular giants. We analyzed the pulsation component in the solar-like counterpart, and the results will be published elsewhere. The analysis of the only three sdBVs we found in NGC6791 has been already reported by Sanjayan *et al.* (2022). Among sdBVs only *Gaia* EDR3 2051105509596144768 is a known binary star. The RV is likely influenced by orbital motion. The other two sdBVs also show different RVs from the cluster average, which may be an indication of their binary nature. Sanjayan *et al.* (2022) reported on the time-series spectroscopy (their Figure 4), which indicates a RV variation. The RVs of other pulsators we found to be members of NGC 6791 are close to the average value, with only a few exceptions. For instance, *Gaia* EDR3 2051293255503478528 shows a much faster motion, but the quality flag of the spectra suggests a possible contamination. We do not have resources to sort out these inconsistency cases. Perhaps the explanation of these cases is an additional RV component either of a binary or a rotational nature. In the case of other objects the RV confirms their membership and a single nature. We are aware that their spectra could have been taken while their orbital RV is negligible, but we consider it to be a less likely case. As in the case of binaries, the location of pulsators in the CMD (the middle panels of Fig. 3 and 6) may still be influenced by binary components.

### 5.3 Rotational Variables

We defined rotational type as stars showing modulated flux variation. Such variation is caused by the presence of migrating spots on the surface, which contribute to a flux modulation as a star rotates. The rotational variables can mimic other types of variability, e.g. ellipsoidal or contact binaries, and high-amplitude radially pulsating stars. We stress that our identification may not be ideal for rotational variable stars. We assumed that binaries show none or negligible modulation of a flux variation. This modulated variation can be verified by either a light curve shape or a profile of peaks in amplitude spectra. A complex profile indicates either period or amplitude change. Objects showing light curves with modulated flux variation have been classified as rotational variables.

We found a total of 145 rotational variables out of which 62 are cluster members and are listed in Table 3. The field counterpart is listed in Table 7. Likewise among binaries, there is no *Gaia* astrometry for four rotational variables and they are also listed in Table 7. We show the CMD location of members in the bottom panel of Fig. 3. The members occupy mostly the MS region, with three exceptions being the RGB objects and three exceptions being BS objects. Likewise in the case of binaries and pulsators, their true location may be influenced by binarity.

Table 2: List of cluster members showing pulsations. See the caption of Table 1 for explanation. Ref 6 refers to Sanjayan *et al.* (2022).

<i>Gaia</i> EDR3	KIC	G [mag]	CMD	HRD	T <sub>eff</sub> [K]	logg	RV [km/s]	[Fe/H]	Ref
$\gamma$ -Dor									
2051105479535706752	2438249 <sup>17L</sup>	15.573	BS	BS	6 980(90)	3.636(84)	-56.7(9)	-0.15(13)	2*
solar-like									
2051098710667044608	2297384 <sup>17L</sup>	14.204	RC	RC	4 512(91)	2.460(28)	-45.71(17)	0.400(7)	5
2051099260422933632	2437539 <sup>17L</sup>	14.545	RGB	RGB	4230(30)	2.353(10)	-39.9(4)	-0.57(7)	2*
2051099329142406400	2437240 <sup>17L</sup>	14.648	RGB	RGB	4 380(70)	3.116(17)	-45.5(3)	-0.12(13)	2*
<b>2051104586182496000</b>	2438462 <sup>12L</sup>	14.586	RGB	RGB	4 240(80)	2.020(23)	-45.71(37)	-0.39(7)	2*
2051105135938204160	2437507 <sup>17L</sup>	14.032	RGB	RGB	4 262(80)	2.160(46)	-47.504(21)	0.400(7)	5
2051105135938218624	2437698 <sup>17L</sup>	14.191	RC	RC	4 521(93)	2.370(28)	-45.25(6)	0.400(8)	4
2051105239017444992	2437564 <sup>17L</sup>	14.226	RC	RC	4 515(99)	2.400(29)	-48.53(11)	0.400(9)	5
2051105342096702080	2437804 <sup>17L</sup>	14.110	RC	RC	4 459(97)	2.350(27)	-45.367(23)	0.400(9)	5
2051286795872609920	2436209 <sup>17L</sup>	14.802	RGB	RGB	4 498(103)	2.650(45)	-47.91(45)	0.400(9)	5
<b>2051287002031072768</b>	2437164 <sup>12L</sup>	14.157	RC	RC	4 300(50)	2.515(10)	-48.26(37)	-0.58(13)	2*
2051287070750544128	2436900 <sup>17L</sup>	14.456	RGB	RGB	4 428(101)	2.500(45)	-47.92(8)	0.400(9)	5
<b>2051287242549228032</b>	2436608 <sup>10L</sup>	14.446	RGB	RGB	4 500(50)	2.254(35)	-45.5(15)	-0.07(7)	2*
<b>2051287311268703232</b>	2436543 <sup>12L</sup>	14.120	RC	-	-	-	-	-	-
2051287311268706432	2436540 <sup>17L</sup>	14.856	RGB	RGB	4 473(104)	2.560(46)	-48.13(14)	0.400(10)	4
2051288067183227008	2436417 <sup>17L</sup>	14.104	RC	-	-	-	-	-	-
2051288135902691840	2436332 <sup>17L</sup>	14.302	RGB	RGB	4 360(60)	3.445(20)	-47.54(30)	-0.07(12)	2*
2051288170262450816	2436458 <sup>17L</sup>	14.532	RGB	RGB	4 250(30)	2.602(10)	-46.36(30)	-0.24(11)	2*
2051291228279110912	2435987 <sup>17L</sup>	14.529	RGB	RGB	4 428(98)	2.490(46)	-44(4)	0.400(9)	5
2051292877546340864	2437340 <sup>17L</sup>	13.462	RGB	RGB	4 058(82)	1.660(43)	-45.0(8)	0.300(9)	5
2051293083704792960	2437444 <sup>17L</sup>	13.998	RGB	RGB	4 105(66)	2.35(11)	-56(4)	0.12(6)	3
2051293118064539520	2437496 <sup>17L</sup>	13.069	RGB	RGB	3 920(67)	1.350(45)	-47.8(7)	0.300(7)	5
2051293118064542976	2437653 <sup>17L</sup>	15.090	RGB	RGB	4 559(97)	2.710(48)	-47(1)	0.400(8)	5
<b>2051293152424246912</b>	2436884 <sup>10L</sup>	13.476	RGB	RGB	4 061(83)	1.670(43)	-44.482(34)	0.300(9)	4
2051293186784001152	2437103 <sup>17L</sup>	14.378	RGB	RGB	4 500(50)	3.356(41)	-48.6(15)	0.002(92)	2*
2051293221143724032	2436824 <sup>17L</sup>	14.478	RGB	-	-	-	-	-	-
2051293221143725952	2436814 <sup>17L</sup>	14.209	RGB	-	-	-	-	-	-
2051293255503469184	2436912 <sup>17L</sup>	14.181	RC	RC	4 330(90)	2.140(46)	-45.75(42)	0.300(8)	4
2051293255503478528	2437040 <sup>17L</sup>	14.158	RGB	RGB	3 760(50)	2.955(27)	-81.7(8)	0.003(10)	5*
2051293319920668160	2569935 <sup>17L</sup>	13.065	RGB	RGB	4 032(65)	1.500(46)	-47.90(8)	0.400(6)	5
2051293599100902016	2570518 <sup>17L</sup>	14.683	RGB	RGB	4 509(89)	2.600(49)	-48.68(8)	0.300(7)	5
2051293977058270592	2436732 <sup>17L</sup>	14.135	RC	RGB	4 300(100)	2.60(7)	-44.9(2)	-0.36(8)	2*
2051294045777739520	2569360 <sup>17L</sup>	14.093	RGB	RGB	4 287(86)	2.180(46)	-46.44(47)	0.300(8)	5
2051294114497261952	2569618 <sup>17L</sup>	14.797	RGB	RGB	4 486(103)	2.650(46)	-45.75(9)	0.400(9)	5
<b>2051294213273828224</b>	2569624 <sup>X</sup>	12.965	RGB	RGB	3 896(62)	1.300(45)	-44.98(7)	0.300(6)	5
<b>2051294251936167424</b>	2569204 <sup>11L</sup>	13.293	RGB	RGB	3 967(77)	1.430(43)	-47.909(11)	0.300(8)	5
2051297275593144192	2569055 <sup>17L</sup>	14.173	RC	RC	4 543(97)	2.450(29)	-46.881(12)	0.400(8)	5
sdBV									
2051105509596144768	2438324 <sup>35S,12L</sup>	17.859	EHB	EHB	25 290(300)	5.510(43)	-90(3)	-2.62(11)	6
2051105754408746880	2437937 <sup>1S,1L</sup>	17.878	EHB	EHB	24 860(270)	5.348(52)	-75(6)	-2.46(12)	6
2051294183216739584	2569576 <sup>12S,5L</sup>	17.752	EHB	EHB	23 540(210)	5.311(35)	-28(4)	-2.73(23)	6
semi-regular									
2051105101578558464	2438151 <sup>17L</sup>	15.655	RGB	MS	5 420(60)	3.912(19)	-50.0(15)	-0.10(9)	1*
2051105616974709504	2438421 <sup>17L</sup>	12.246	AGB	AGB	3 555(57)	0.510(43)	-46.540(46)	0.200(8)	5
2051287002031070208	2437171 <sup>17L</sup>	12.394	AGB	AGB	3 540(56)	0.610(42)	-47.11(16)	0.300(8)	5
2051287173829740032	2436324 <sup>8L</sup>	12.373	AGB	AGB	3 332(53)	0.270(41)	-49.315(19)	0.200(10)	5
2051292976324527232	2437317 <sup>17L</sup>	14.939	RGB	-	-	-	-	-	-

Table 3: List of cluster members showing rotational variability. See the caption of Table 1 for explanation.

<i>Gaia</i> EDR3	KIC	Period [days]	G [mag]	CMD	HRD	$T_{\text{eff}}$ [K]	logg	RV [km/s]	[Fe/H]	Ref
2051099015605500672	2297584 <sup>X</sup>	18.02	18.299	MS+	–	–	–	–	–	–
2051104757981275264	2438685 <sup>X</sup>	7.78	17.256	RGB	MS	5 500(50)	4.953(20)	-44.8(44)	0.47(15)	1 *
<b>2051104891118311040</b>	2437994 <sup>X</sup>	1.85	19.228	MS+	–	–	–	–	–	–
<b>2051104891120796672</b>	2437990 <sup>X</sup>	13.15	19.148	MS+	–	–	–	–	–	–
2051104959840285696	2437791 <sup>X</sup>	15.28	18.067	MS+	–	–	–	–	–	–
<b>2051104964139549824</b>	2437941 <sup>X</sup>	10.12	17.944	MS	–	–	–	–	–	–
2051104994200024448	2438113 <sup>X</sup>	5.80	17.288	MS	–	–	–	–	–	–
2051105097281783040	2438031 <sup>X</sup>	8.28	17.591	MS	MS	5 810(40)	4.216(34)	-62.3(23)	-0.158(47)	1 *
2051105131636983808	2437646 <sup>X</sup>	13.23	17.558	MS	–	–	–	–	–	–
2051105234715895552	2437707 <sup>X</sup>	11.00	17.867	MS	MS	6 080(30)	4.641(35)	-47.8(48)	0.60(14)	1 *
2051105273377206784	2437801 <sup>X</sup>	7.19	18.508	MS+	MS	5 380(70)	4.111(26)	-65.30(10)	-0.40(10)	1 *
<b>2051105342091728384</b>	2437761 <sup>X</sup>	11.81	19.001	MS	–	–	–	–	–	–
2051105372154852736	2437849 <sup>4L</sup>	11.02	16.863	MS	MS	5 260(50)	3.923(16)	-51.7(14)	-0.31(11)	1 *
2051105372154855552	2437944 <sup>X</sup>	1.96	18.543	MS+	–	–	–	–	–	–
<b>2051105372157195264</b>	–	2.45	19.556	MS+	MS	5480(50)	4.835(21)	-56(4)	0.45(17)	1 *
2051105578318626304	2438569 <sup>X</sup>	7.00	17.279	MS	MS	5 970(50)	4.295(20)	-69.2(15)	0.32(14)	1 *
<b>2051105612675379968</b>	2438390 <sup>X</sup>	3.80	17.987	MS	–	–	–	–	–	–
<b>2051105685689315968</b>	2438129 <sup>X</sup>	16.58	17.853	MS	–	–	–	–	–	–
2051105784484742144	2570443 <sup>X</sup>	2.20	17.643	MS	MS	5 610(50)	4.298(20)	-133.2(45)	-0.62(30)	1 *
<b>2051105818833811584</b>	2438344 <sup>X</sup>	7.74	18.616	MS+	–	–	–	–	–	–
2051105857492894592	2570649 <sup>X</sup>	13.36	17.293	MS	–	–	–	–	–	–
<b>2051105921913036160</b>	2570622 <sup>X</sup>	9.57	19.026	MS+	–	–	–	–	–	–
<b>2051105926212896512</b>	2570559 <sup>X</sup>	1.32	20.343	MS+	–	–	–	–	–	–
<b>2051107055787471104</b>	2438631 <sup>X</sup>	7.36	19.729	MS+	–	–	–	–	–	–
<b>2051287002024520064</b>	–	10.86	19.640	MS+	–	–	–	–	–	–
<b>2051287066449451136</b>	2436942 <sup>X</sup>	9.26	18.098	MS	–	–	–	–	–	–
2051287066449464064	2436959 <sup>X</sup>	2.65	18.852	MS+	–	–	–	–	–	–
2051287070744003456	2436969 <sup>X</sup>	7.92	19.132	MS+	RGB	4 500(50)	3.09(8)	-45.0(8)	-0.155(20)	2 *
2051287242549232384	2436767 <sup>X</sup>	12.32	17.309	MS	MS	5 690(50)	4.163(20)	-43.2(57)	0.148(33)	1 *
<b>2051287895379273088</b>	2436011 <sup>X</sup>	10.00	19.632	MS+	–	–	–	–	–	–
2051288372119657728	2569185 <sup>X</sup>	13.43	17.258	MS	MS	5 660(50)	4.117(34)	-97.9(35)	-0.08(10)	1 *
2051288376420896384	2569162 <sup>X</sup>	5.90	18.088	MS	–	–	–	–	–	–
2051291262638872192	2568864 <sup>X</sup>	14.42	17.618	MS	MS	5 370(30)	4.78(10)	-61.5(42)	0.58(27)	1 *
<b>2051291503157017472</b>	2568685 <sup>X</sup>	19.87	17.342	MS	–	–	–	–	–	–
2051292873245240192	2437350 <sup>X</sup>	16.82	17.885	MS	MS	5 790(50)	4.913(20)	-74.3(15)	0.13(8)	1 *
<b>2051292911906089728</b>	2437521 <sup>X</sup>	11.27	17.987	MS+	–	–	–	–	–	–
<b>2051292946259301504</b>	2437092 <sup>2L</sup>	3.20	18.145	MS+	MS	4 700(100)	4.619(50)	-78(1)	-1.87(6)	1 *
2051293014978876672	2437584 <sup>X</sup>	5.90	18.486	–+	–	–	–	–	–	–
2051293083704791040	2437354 <sup>8L</sup>	7.21	16.465	MS	MS	5 580(50)	4.391(20)	-55.6(8)	-0.413(46)	2 *
2051293113776412416	2437613 <sup>X</sup>	11.05	17.787	MS	–	–	–	–	–	–
2051293148133456896	2437062 <sup>X</sup>	8.82	17.133	RGB	–	–	–	–	–	–
2051293152424243968	2436909 <sup>X</sup>	12.00	16.778	MS	MS	5 640(40)	4.654(21)	-69.3(26)	-0.203(17)	1 *
2051293186783997056	–	9.63	18.232	MS+	–	–	–	–	–	–
<b>2051293186784004096</b>	2437238 <sup>X</sup>	4.00	16.079	BS	BS	5 880(30)	3.546(23)	-48.0(4)	-0.34(8)	2 *
<b>2051293255503480320</b>	2437079 <sup>X</sup>	5.81	16.794	BS	–	–	–	–	–	–
<b>2051293289863230720</b>	2437338 <sup>X</sup>	1.24	16.655	BS	–	–	–	–	–	–
2051293319934813184	2569984 <sup>X</sup>	12.50	17.704	MS	–	–	–	–	–	–
2051293358583014528	2569763 <sup>4L</sup>	8.29	16.648	MS	MS/RGB	5 510(20)	3.788(49)	-38.6(5)	-0.397(48)	2 *
2051293392942762240	2569825 <sup>X</sup>	0.48	18.754	MS+	MS	5 000(50)	4.86(15)	-86.3(7)	0.02(14)	1 *
2051293427302195584	2437884 <sup>X</sup>	3.23	16.871	MS+	MS	5 930(20)	4.048(26)	-43.9(3)	-0.44(10)	2 *
2051293530375009920	2570217 <sup>X</sup>	5.55	17.891	MS	MS	5 760(20)	4.49(7)	-62.4(23)	0.07(8)	1 *
2051293663519464192	2570420 <sup>X</sup>	19.96	17.951	MS	–	–	–	–	–	–
2051293977053182592	2436790 <sup>X</sup>	9.61	18.861	MS	MS	4 990(80)	4.832(25)	-169(3)	-0.356(15)	1 *
<b>2051294007116759808</b>	2569597 <sup>X</sup>	7.17	18.091	MS+	–	–	–	–	–	–
<b>2051294148851985536</b>	–	9.66	20.397	MS+	–	–	–	–	–	–
<b>2051294148857020160</b>	2569767 <sup>X</sup>	2.40	17.323	MS+	–	–	–	–	–	–
2051294217574157440	–	4.92	19.300	MS+	–	–	–	–	–	–
<b>2051294251931077888</b>	2569279 <sup>X</sup>	1.14	18.883	MS+	–	–	–	–	–	–
<b>2051294281994746880</b>	2569324 <sup>X</sup>	10.90	17.983	MS	–	–	–	–	–	–
2051294286296294528	2569334 <sup>X</sup>	6.29	17.447	MS	MS	5 330(20)	4.220(25)	-47.4(23)	0.15(8)	1 *
2051294797390943872	2569591 <sup>X</sup>	14.89	17.679	MS	–	–	–	–	–	–
<b>2051296176081696768</b>	2570281 <sup>12L</sup>	14.42	14.785	RGB	–	–	–	–	–	–

Table 4: List of cluster members with unclassified variability. See the caption of Table 1 for explanation.

<i>Gaia</i> EDR3	KIC	Period [days]	G [mag]	CMD	HRD
2051105269075634176	2437760 <sup>X</sup>	0.44	18.064	MS	–
<b>2051288067182949760</b>	2436421 <sup>8L</sup>	1.44	14.937	BS	–
<b>2051291498855854208</b>	2568724 <sup>X</sup>	0.63	20.141	MS <sup>+</sup>	–
<b>2051293049345064832</b>	2437745 <sup>X</sup>	1.43	15.968	BS	–
<b>2051294148857016192</b>	2569676 <sup>X</sup>	0.27	18.037	MS <sup>+</sup>	–

#### 5.4 Unclassified and unidentified variables

In the case of nine objects, we were unable to unambiguously classify them according to the three types described above. The amplitude of a flux variation is low and it is not clear if the variation remains stable over time. The latter indicates that it is not unlikely these stars may be rotational variables. We leave a definite classification for further analysis, preferentially if based on better quality data. Five members of the cluster are listed in Table 4 and they are plotted in the bottom panel of Fig. 3, while four non-members are listed in Table 8.

While checking the pixel content we found signals in the amplitude spectra, associated with optical detections found in Pan-STARRS data (Chambers *et al.* 2016, Flewelling *et al.* 2020) survey that do not have any designations. We classified the signal to a proper variability type and estimated its period. We show the list of these unidentified objects in Table 9. Since the stars are not listed in the *Gaia* catalog, we are unable to estimate their membership. At three locations on the silicon (last three coordinates listed), we detected a signal in the amplitude spectra, however, we are unable to associate these coordinates with any optical objects in the Pan-STARRS survey. In addition, the last two signals listed may be of the same origin, though the coordinates are different. This result indicates that these three signals listed are residual signals of some other variable stars in the *Kepler* field of view that were spread over the silicon. We consider the signals detected at those three specific locations on the detector to be artifacts and not real sources.

## 6. The distance and age estimation

We downloaded a grid of isochrones given in the *Gaia* photometric system from the MESA Isochrones and Stellar Tracks (MIST) project (Choi *et al.* 2016, Dotter 2016). The current version of MIST is 1.2. The MESA version 7503 was employed to calculate isochrones. We selected  $V/V_{\text{crit}} = 0$ . The grid covers age in a logarithmic scale between 9.8 and 10.3 with a step of 0.01, while  $[\text{Fe}/\text{H}]$  was between 0.20 and 0.45 with a step of 0.01.



At least 50% of the stars are expected to be in binary systems. The observed magnitude of a given target may include the flux contribution from all companions and not a single star, which shifts the position of the target in the CMD. Therefore, we excluded outlying stars where their positions in the CMD are uncertain. For the fit, we only kept the MS, RGB and RC stars. We included magnitude uncertainties as weights in the fit, which prevented the MS targets from over-fitting. The RC and RGB targets, even though less numerous, are brighter, and hence also remains significant in the fit.

The MIST synthetic isochrones are given in absolute magnitudes, and we selected no extinction. To account for a distance and a non-vacuum environment, in our fit, we included a shift ( $m-M$ ) in the *Gaia* G magnitude and in  $B_p-R_p$  color. The best-fit isochrones point to a narrow range of age and  $[Fe/H]$ . The age is 8.91 Gyr, while  $[Fe/H]$  is between 0.26 and 0.28. The apparent distance modulus ( $m-M$ ) equals 13.424, while  $E(B_p-R_p)$  from 0.165 to 0.176. We show the fits in Fig. 5. Based on the extinction curve from Cardelli *et al.* (1989), Bressan *et al.* (2012) showed a rough relation between extinction in the *Gaia* G band and  $E(B_p-R_p)$ , which is  $A_G \approx 2 \cdot E(B_p-R_p)$ . Taking the average of  $E(B_p-R_p)=0.171$  and using this relation, we derived  $A_G=0.342$  mag. Subtracting  $A_G$  from ( $m-M$ ) we find the true distance modulus of 13.082, which gives the distance to the cluster of 4134 pc. We also derived distance from the parallaxes of the cluster members with probability membership at least 90% and the relative parallax uncertainty of smaller than 10%, which equals 4123(31) pc. The distance estimated from the isochrone fit lies well within the uncertainty of the distance estimations from the cluster parallax. The cluster age we derived from the isochrone fit is also comparable to the age reported by Choi *et al.* (2018).

To verify the correctness of the spectroscopic fits we also engaged isochrones in  $T_{\text{eff}}$  and  $\log g$  plane (HRD). We used the isochrones for the age and the average metallicity, which we derived from the isochrone fitting in the CMD. Then, we overplotted the isochrones with our variable stars from Tables 1-3, for which  $T_{\text{eff}}$  and  $\log g$  are listed. The column 'HRD' in Tables 1-3 describes the location of a given star in the HRD. If the location agrees with the one in CMD, we can expect the spectroscopic fit is likely correct and we obtained an agreement for the majority of stars. It should be noted that the scatter in the HRD is larger, hence some objects may have not been allocated properly. There are clear exceptions, eight among binaries, two among pulsators and two among rotational variables. These cases should be treated with caution.

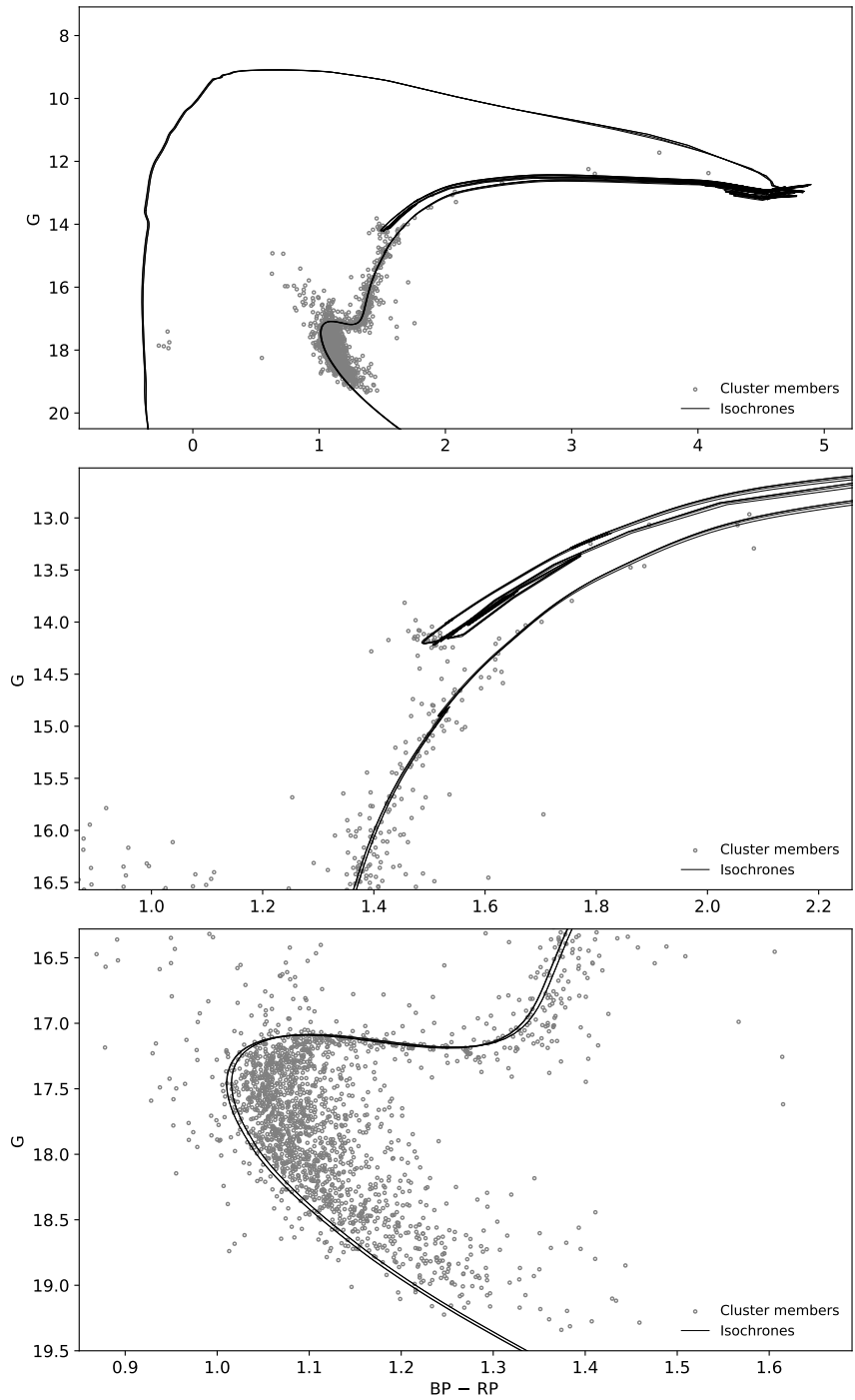


Figure 5: The color-magnitude diagram of NGC 6791, showing the best MIST isochrone fits. The top panel shows the overall diagram, while the middle panel shows the red clump region and the bottom panel shows the main-sequence region.

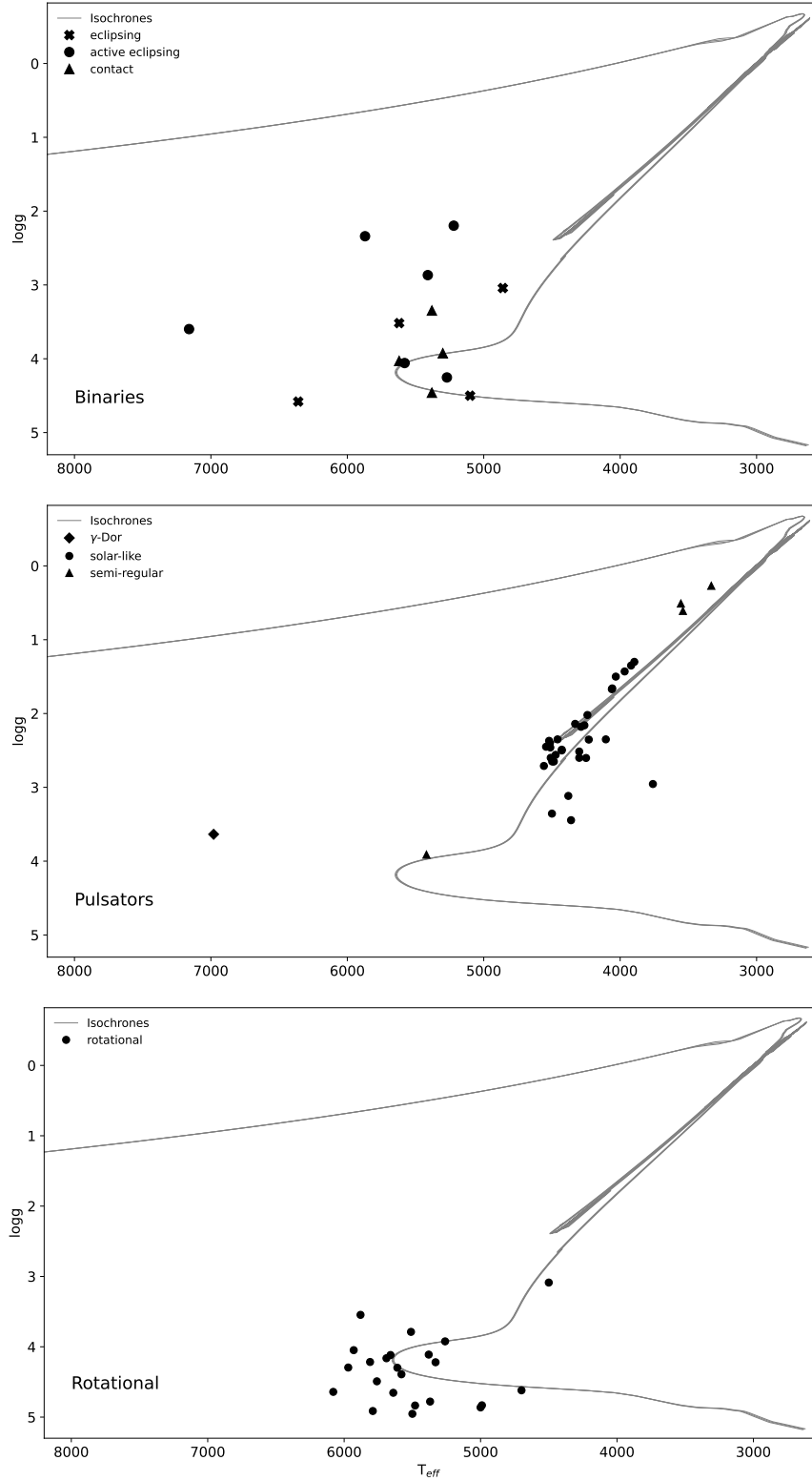


Figure 6: The  $T_{\text{eff}}$ – $\log g$  diagram showing the cluster members with atmospheric parameters derived in this work. The top, middle and bottom panels show binary, pulsating and rotational stars, respectively. The isochrones represent the best MIST fits in  $T_{\text{eff}}$  and  $\log g$  coordinates.

Table 5: List of binary stars that are not cluster members. See the caption of Table 1 for explanation. Targets with no astrometry available, hence with no membership established, are denoted in *italic*.

<i>Gaia</i> EDR3	KIC	P <sub>orb</sub> [days]	T <sub>0</sub> [BJD]	G [mag]	T <sub>eff</sub> [K]	logg	RV [km/s]	[Fe/H]	Ref
eclipsing									
<b>2051104826700758016</b>	2438661 <sup>X</sup>	196.34051(1)	2 455 037.21466(43)	16.449	–	–	–	–	–
2051105131638986752	–	23.878352(36)	2 454 967.0873(12)	19.782	–	–	–	–	–
2051107128803742336	2438562 <sup>X</sup>	10.406512(6)	2 454 965.58747(47)	19.369	6 220(130)	2.864(51)	-49(4)	-1.29(17)	2*
2051287311268711168	2436579 <sup>X</sup>	9.287153(22)	2 454 971.1134(18)	19.613	–	–	–	–	–
2051291739386261248	2568780 <sup>X</sup>	3.5316020(11)	2 454 964.71245(25)	19.913	–	–	–	–	–
2051292907615354240	2437452 <sup>1S,17L</sup>	14.4699358(24)	2 454 974.81692(14)	17.286	6 170(50)	4.26(9)	-92.1(6)	-0.86(9)	2*
2051293079414230912	2437505 <sup>10L</sup>	21.476420(11)	2 454 982.26244(40)	18.324	4 920(50)	3.25(6)	-19.6(30)	-0.25(19)	1*
<b>2051293118063233408</b>	2437675 <sup>X</sup>	1.75	–	21.175	–	–	–	–	–
<b>2051294629893394176</b>	2569880 <sup>X</sup>	0.51323254(22)	2 454 964.60382(35)	17.866	–	–	–	–	–
active eclipsing									
2051104586182512128	2438502 <sup>6S,16L</sup>	8.35905(26)	2 455 005.2748(14)	16.216	5 563(234)	4.17(37)	-14(5)	0.37(22)	3
2051104684959920896	2438464 <sup>X</sup>	0.43657907(7)	2 454 964.92853(13)	19.443	4 310(50)	4.169(20)	41(16)	-0.91(6)	1*
<b>2051286761512868992</b>	2436203 <sup>X</sup>	2.06	–	14.328	–	–	–	–	–
2051288170257319808	–	3.7024382(14)	2 454 968.16622(31)	20.135	–	–	–	–	–
2051288372119654528	2569138 <sup>X</sup>	0.88305272(12)	2 454 964.71084(11)	19.205	–	–	–	–	–
2051293599094508032	–	2.8516350(19)	2 454 967.1274(6)	20.335	–	–	–	–	–
contact									
2051105543955885312	2438471 <sup>X</sup>	0.27345629(34)	2 454 964.8195(11)	19.527	4 300(50)	3.92(7)	3.9(9)	-1.354(25)	1*
2051288269040355584	2436044 <sup>X</sup>	0.24533697(21)	2 454 964.6646(7)	19.452	–	–	–	–	–
<b>2051286417915483392</b>	2297170 <sup>X</sup>	0.3664306(6)	2 455 002.6182(13)	17.797	–	–	–	–	–
2051287070750548736	2437038 <sup>17L</sup>	0.267678275(46)	2 454 964.58218(14)	16.149	–	–	–	–	–
2051291228279113216	2435971 <sup>17L</sup>	0.27182769(8)	2 454 964.81810(25)	16.276	–	–	–	–	–
2051291468797350528	2568971 <sup>17L</sup>	5.088522(10)	2 454 966.2350(17)	13.081	–	–	–	–	–
2051293530381417856	2570289 <sup>17L</sup>	0.279027932(31)	2 454 964.57880(1)	15.781	–	–	–	–	–
<b>2051295076563264000</b>	2570552 <sup>X</sup>	0.28417822(44)	2 454 964.5913(13)	20.279	–	–	–	–	–
2051295454527201792	2570460 <sup>X</sup>	0.2659879(15)	2 454 964.61531(47)	18.689	–	–	–	–	–
2051296313520692864	2708123 <sup>X</sup>	0.302184513(81)	2 454 964.69239(22)	17.742	–	–	–	–	–
2051297374371300992	2569082 <sup>X</sup>	0.33401898(23)	2 454 964.8252(6)	17.579	5 750(50)	4.052(15)	-38.30(54)	-1.069(20)	1*
<b>2051297477460338304</b>	–	0.2690446(1)	2 454 964.7175(30)	20.838	–	–	–	–	–
outbursting									
2051287203888388736	2436450 <sup>15S,12L</sup>	35.71	–	19.884	–	–	–	–	–

## 7. Summary

We presented a search for variable stars in the *Kepler* superstamp data. All available pixels were searched, by means of a Fourier amplitude spectrum, and a contiguous optimal aperture for each object that shows a significant flux variation were defined. The coordinates of these optimal apertures were matched with optical counterparts using Pan-STARRS. In total, we detected 278 variable stars. We cross-matched our variable star sample with those reported in the literature and found 16 variable stars reported by Kaluzny and Rucinski (1993), four by Rucinski *et al.* (1996), 23 by Mochejska *et al.* (2002), six by Mochejska *et al.* (2003), four by Kaluzny (2003), 15 by Bruntt *et al.* (2003), seven by Mochejska *et al.* (2005), one by Hartman *et al.* (2005) and 33 by de Marchi *et al.* (2007). We found 240 stars having KIC designations, out of which 140 stars do not have data delivered to the MAST. A variability of 119 stars was not known prior to our analysis. These stars are marked in bold in Tables 1-8, including the first nine objects listed in Table 9. Just recently, and independently of our work, Colman *et al.* (2022) reported light curves of stars with a KIC designation, however the authors did not specify which stars were found variables, only reporting a total number of 239 variables. Even accounting for this report, which is limited to the KIC stars only, we can consider 26 variable stars having no KIC designation (including seven objects marked in bold), to be new detections. No ground-based work on

Table 6: List of pulsators that are not cluster members. See the caption of Table 1 for explanation.

<i>Gaia</i> EDR3	KIC	G [mag]	T <sub>eff</sub> [K]	logg	RV [km/s]	[Fe/H]	Ref
$\delta$ -scuti							
2051098981244205056	2297728 <sup>1S,18L</sup>	9.929	6 888(25)	3.680(40)	-37(7)	0.272(22)	3
2051107369321426432	2570760 <sup>18L</sup>	13.459	–	–	–	–	–
solar-like							
<b>2051098710667526912</b>	2297357 <sup>1L</sup>	12.115	–	–	–	–	–
<b>2051099054264914048</b>	2437622 <sup>12L</sup>	15.583	–	–	–	–	–
<b>2051099329142404480</b>	2437207 <sup>X</sup>	18.731	–	–	–	–	–
2051104105146054784	2297793 <sup>17L</sup>	13.626	4 085(81)	1.430(52)	-83.615(30)	-0.300(10)	5
2051104139506469760	2438094 <sup>17L</sup>	15.322	4 060(50)	1.11(15)	-84.7(6)	-1.14(8)	2*
2051104861060304640	2437816 <sup>17L</sup>	13.958	4 229(77)	2.090(47)	0.400(7)	-47.27(9)	5
<b>2051105720053903232</b>	2438289 <sup>10L</sup>	14.384	–	–	–	–	–
2051105857492905600	2570715 <sup>7L</sup>	12.678	4 713(84)	2.330(36)	-3.30(7)	-0.200(7)	5
<b>2051107369321441920</b>	2570794 <sup>10L</sup>	15.158	–	–	–	–	–
2051286520994706432	2436457 <sup>18L</sup>	13.245	4 969(24)	3.015(39)	-19.14(4)	-0.422(22)	3
<b>2051286933311578112</b>	2436680 <sup>10L</sup>	15.187	–	–	–	–	–
2051288445140366464	2569078 <sup>10L</sup>	13.650	4 418(90)	2.290(49)	-5.428(56)	0.200(8)	5
2051291434437586304	2568912 <sup>8L</sup>	12.859	4 701(95)	3.01(6)	-7.122(55)	-0.100(8)	5
<b>2051291567575397120</b>	2568656 <sup>X</sup>	15.618	–	–	–	–	–
2051291571876502912	2568654 <sup>11L</sup>	13.140	4 301(83)	2.07(5)	-73.155(12)	0.100(8)	5
2051291674955780992	2568888 <sup>10L</sup>	14.131	4 387(100)	2.070(51)	-58.47(23)	-0.100(11)	5
<b>2051291949833615104</b>	2568575 <sup>5L</sup>	13.407	4 501(50)	2.55(8)	-2.26(4)	0.181(48)	3
2051293118064546944	2437692 <sup>15L</sup>	11.203	4 817(86)	2.610(38)	-12.780(24)	0.200(6)	5
<b>2051293702180102144</b>	2570002 <sup>X</sup>	13.628	–	–	–	–	–
2051294320655654912	2569137 <sup>10L</sup>	13.630	4 298(102)	1.71(6)	-194.10(44)	-0.800(16)	5
<b>2051295282728537216</b>	2570696 <sup>2L</sup>	13.620	4 461(80)	2.13(6)	-11.38(9)	-0.300(8)	5
RRLyrr/BLBoo							
<b>2051294934839887872</b>	2569850 <sup>X</sup>	20.426	–	–	–	–	–
semi-regular							
2051105032859063424	2438242 <sup>X</sup>	16.817	4 511(99)	2.660(47)	-47.85(8)	0.400(9)	4

Table 7: List of rotational variables that are not cluster members. See the caption of Table 1 for explanation.

<i>Gaia</i> EDR3	KIC	Period [days]	G [mag]	T <sub>off</sub> [K]	logg	RV [km/s]	[Fe/H]	Ref
<b>2051098951180105088</b>	—	1.33	20.929	—	—	—	—	—
<b>2051099088624172928</b>	2297416 <sup>X</sup>	2.66	20.201	—	—	—	—	—
2051099187404218752	2436945 <sup>X</sup>	4.58	16.735	—	—	—	—	—
<b>2051104139500783744</b>	—	0.64	20.943	—	—	—	—	—
2051104139505811328	2297846 <sup>X</sup>	13.40	14.901	—	—	—	—	—
<b>2051104272645525760</b>	2438284 <sup>X</sup>	2.63	19.629	—	—	—	—	—
<b>2051104272645529472</b>	—	1.53	20.277	—	—	—	—	—
2051104276944815744	2438272 <sup>18L</sup>	11.48	13.173	—	—	—	—	—
2051104586182508928	2438513 <sup>15S,17L</sup>	13.27	13.939	5 652(125)	4.51(8)	-35.74(33)	0.000(10)	5
<b>2051104753679401728</b>	2438740 <sup>X</sup>	0.42	19.653	—	—	—	—	—
2051104826696024832	—	1.06	20.370	—	—	—	—	—
2051104925480543616	2437773 <sup>X</sup>	0.51	19.083	6 070(110)	2.9(1)	8(4)	-0.54(15)	2*
<b>2051105062917626624</b>	2437959 <sup>X</sup>	15.27	17.987	—	—	—	—	—
<b>2051105067218772096</b>	2437888 <sup>8L</sup>	10.34	14.730	6 120(80)	4.93(5)	16.42(37)	-0.39(12)	2*
<b>2051105067218785280</b>	2438003 <sup>18L</sup>	0.70	13.025	7 132(30)	4.102(50)	3(10)	-0.22(3)	3
<b>2051105135933158144</b>	—	3.99	20.627	—	—	—	—	—
<b>2051105239017448448</b>	2437649 <sup>X</sup>	7.62	16.377	—	—	—	—	—
<b>2051105273377200384</b>	2437789 <sup>X</sup>	16.61	17.023	—	—	—	—	—
<b>2051105303437700224</b>	2437984 <sup>X</sup>	4.70	19.703	—	—	—	—	—
2051105307736986496	2437996 <sup>17L</sup>	14.61	13.887	5 753(37)	4.60(6)	-38(5)	0.104(35)	3
2051105410811376640	2438305 <sup>X</sup>	7.01	19.692	—	—	—	—	—
<b>2051105823133141888</b>	2438376 <sup>X</sup>	11.44	17.788	—	—	—	—	—
<b>2051105926207653504</b>	—	5.11	20.540	—	—	—	—	—
<b>2051106063646757888</b>	2438861 <sup>X</sup>	1.48	19.672	—	—	—	—	—
2051107124503872256	2438516 <sup>X</sup>	5.13	18.313	5 150(50)	4.773(27)	-36.9(15)	0.64(30)	1*
2051107472400670720	2570846 <sup>17L</sup>	10.82	15.313	—	—	—	—	—
2051107541120138752	2570736 <sup>X</sup>	1.61	18.428	—	—	—	—	—
<b>2051286997729896832</b>	—	0.86	19.542	—	—	—	—	—
2051287066448488192	—	1.62	19.279	4 850(50)	4.871(40)	-112.4(1)	-0.15(12)	1*
2051287139470009088	2436635 <sup>17L</sup>	1.17	15.989	4 445(291)	4.09(45)	-76(6)	-0.32(27)	3
<b>2051287547485746432</b>	2436206 <sup>X</sup>	8.25	17.626	—	—	—	—	—
<b>2051288032823472128</b>	2436274 <sup>X</sup>	4.58	18.220	—	—	—	—	—
<b>2051288101537860992</b>	—	3.39	20.539	—	—	—	—	—
<b>2051288165961197952</b>	2436416 <sup>X</sup>	3.99	19.859	—	—	—	—	—
<b>2051288445135225472</b>	2569015 <sup>X</sup>	1.32	20.103	—	—	—	—	—
<b>2051290919041461632</b>	2435889 <sup>X</sup>	14.47	16.670	—	—	—	—	—
<b>2051291434437576320</b>	2568884 <sup>X</sup>	10.50	18.224	—	—	—	—	—
<b>2051291468792223104</b>	—	7.37	20.190	—	—	—	—	—
<b>2051291571876503424</b>	2568672 <sup>X</sup>	18.09	16.477	—	—	—	—	—
2051292976335015296	2437180 <sup>X</sup>	4.07	17.907	—	—	—	—	—
2051292980625560448	2437292 <sup>X</sup>	5.51	18.356	—	—	—	—	—
2051292980625569792	2437234 <sup>17L</sup>	24.10	13.153	—	—	—	—	—
<b>2051293014978879744</b>	2437723 <sup>X</sup>	1.17	18.608	—	—	—	—	—
<b>2051293014985313152</b>	2437469 <sup>X</sup>	9.85	19.161	—	—	—	—	—
2051293014985313792	2437574 <sup>X</sup>	11.683	17.183	5 650(50)	4.5(8)	-45.0(3)	0.05(7)	1*
<b>2051293049338645504</b>	—	1.97	20.310	—	—	—	—	—
2051293083704793856	2437359 <sup>17L</sup>	16.91	14.598	—	—	—	—	—
<b>2051293152424251648</b>	2436988 <sup>X</sup>	4.69	20.213	—	—	—	—	—
<b>2051293221143720832</b>	2436808 <sup>X</sup>	4.94	16.764	—	—	—	—	—
<b>2051293255503475200</b>	2436958 <sup>X</sup>	4.50	20.342	—	—	—	—	—
2051293289863227520	2437329 <sup>16L</sup>	11.67	15.925	—	—	—	—	—
2051293358577984768	—	1.55	20.049	—	—	—	—	—
<b>2051293388640138880</b>	—	8.48	20.028	—	—	—	—	—
<b>2051293496015260416</b>	2570182 <sup>X</sup>	1.99	18.719	—	—	—	—	—
<b>2051293530375018112</b>	—	4.27	20.832	—	—	—	—	—
2051293599094510848	2570536 <sup>17L</sup>	10.03	14.507	—	—	—	—	—
2051293839619440640	2570259 <sup>15S,1L</sup>	3.84	16.128	—	—	—	—	—
<b>2051293908333956352</b>	2570154 <sup>X</sup>	6.39	18.171	5 380(50)	4.004(20)	-68.6(36)	0.12(8)	1*
2051293942698672000	2570258 <sup>X</sup>	7.40	16.852	—	—	—	—	—
<b>2051293942698685056</b>	2570313 <sup>X</sup>	1.39	19.449	—	—	—	—	—
2051293972756992384	2436621 <sup>X</sup>	7.58	18.758	—	—	—	—	—
2051293977053154688	2436734 <sup>X</sup>	1.59	20.187	—	—	—	—	—
<b>2051294011418019072</b>	2436852 <sup>X</sup>	3.31	18.871	—	—	—	—	—
<b>2051294080137491968</b>	2569421 <sup>X</sup>	13.51	18.689	—	—	—	—	—
<b>2051294114495072896</b>	—	3.54	20.960	—	—	—	—	—
<b>2051294148851973888</b>	2569675 <sup>X</sup>	5.24	20.253	—	—	—	—	—
2051294148857011712	2569737 <sup>14L</sup>	13.54	16.109	—	—	—	—	—
<b>2051294492454406272</b>	2569431 <sup>X</sup>	2.49	17.007	—	—	—	—	—
<b>2051294664251895808</b>	—	4.90	21.163	—	—	—	—	—
2051294728671468672	2569908 <sup>X</sup>	6.32	16.820	—	—	—	—	—
<b>2051294831750674944</b>	2569761 <sup>X</sup>	1.99	20.008	—	—	—	—	—
2051294870413630208	2569467 <sup>X</sup>	9.78	15.965	—	—	—	—	—
2051295007845559552	—	6.08	20.344	—	—	—	—	—
<b>2051295007845583744</b>	—	1.80	21.103	—	—	—	—	—
<b>2051295488886958592</b>	2570555 <sup>X</sup>	6.35	16.869	—	—	—	—	—
<b>2051295557606451456</b>	2570581 <sup>X</sup>	16.52	16.997	—	—	—	—	—
2051296652817037056	2707961 <sup>X</sup>	8.00	18.949	—	—	—	—	—
2051297516106367232	—	2.65	21.041	—	—	—	—	—
<b>2051297962788050816</b>	2707771 <sup>X</sup>	0.73	18.021	—	—	—	—	—
<b>2051298031507519616</b>	2707692 <sup>X</sup>	2.50	19.376	—	—	—	—	—
<b>2051299474616582912</b>	2707858 <sup>X</sup>	0.91	20.076	—	—	—	—	—
2051297275593155328	2569073 <sup>X</sup>	14.66	14.236	—	—	—	—	—
<b>2051293255496998912</b>	—	9.00	19.651	—	—	—	—	—

Table 8: List of unclassified variables that are not cluster members. See the caption of Table 1 for explanation.

<i>Gaia</i> EDR3	KIC	Period [days]	G [mag]	T <sub>eff</sub> [K]	logg	RV [km/s]	[Fe/H]	Ref
2051104654901977984	2438433 <sup>X</sup>	0.93	20.356	–	–	–	–	–
<b>2051105307732052864</b>	2438028 <sup>2L</sup>	0.06	20.639	3 470(50)	3.842(47)	-48.80(30)	0.09(10)	1*
<b>2051288337759883648</b>	2436293 <sup>X</sup>	0.20	18.578	–	–	–	–	–
<b>2051293736533447424</b>	2570195 <sup>X</sup>	0.77	20.856	–	–	–	–	–

Table 9: A list of equatorial coordinates that are associated with superstamp pixels showing signal in their amplitude spectra. In the case of the last three positions listed, we found no optical objects that could be a source of the signal.

$\alpha_{2000}$ [hh mm ss.ss]	$\delta_{2000}$ [dd mm ss.s]	Period [days]	Type
19 20 51.72	+37 47 45.4	1.10	rotational
<b>19 20 53.56</b>	<b>+37 47 05.4</b>	1.20	eclipsing
<b>19 20 56.85</b>	<b>+37 47 43.2</b>	2.40	rotational
19 21 13.06	+37 42 36.3	0.25	binary
<b>19 20 31.99</b>	<b>+37 47 42.4</b>	0.41	binary
<b>19 20 45.84</b>	<b>+37 47 04.1</b>	3.07	rotational
<b>19 20 47.82</b>	<b>+37 42 18.2</b>	0.68	rotational
<b>19 21 03.71</b>	<b>+37 44 17.6</b>	11.68	rotational
<b>19 20 51.85</b>	<b>+37 39 51.5</b>	9.21	solar-like
19 20 32.77	+37 43 23.8	0.15	binary
19 20 44.47	+37 40 51.5	5.73	rotational
19 20 46.46	+37 40 18.9	5.73	rotational

the detection of the variability of these 26 stars was reported, either.

Using *Gaia* EDR3 astrometry, we calculated the membership probabilities for all variable stars in our sample by applying Bayesian Gaussian mixture models. A star is considered to be a cluster member if the probability is higher than 50%. In total, we found 129 variable stars that are cluster members, 17 binary systems, 45 pulsators, 62 rotationally and five unclassified variables. The locations of these cluster variable stars in the CMD diagram were estimated and indicate the evolutionary status of cluster members. In the CMD, a majority of our variable stars are located in the MS. Solar-like pulsators are mostly located in the RGB and RC, while semi-regular variables are located in the RGB and AGB. In addition there are five BS and three EHB stars in the CMD.

In the case of binary systems, we estimated mid-times of eclipses and derived ephemerides. We calculated the O-C diagrams and checked for any orbital period variation. Only three binary systems show significant period variation, however its nature is not confirmed. The solar-like counterpart has been a subject of a detailed analysis of its pulsation content, and the results will be published elsewhere. The analysis of three sdBVs is already reported by Sanjayan *et al.* (2022). The rotational variables are not subject to our detailed analysis. This type of variables can be very useful toward gyrochronology.

We utilized public and archived spectra for 111 variable stars. Spectra for 64 stars were fitted with XTGRID, while for the remainder of the sample, we adopted the fit values from the surveys. We derived  $T_{\text{eff}}$ ,  $\log g$ ,  $[\text{Fe}/\text{H}]$  and RVs. Our spectral analysis was able to recover consistent stellar parameters from very diverse spectroscopic data. This consistency is reflected by the similar distribution of stars in the CMD and HRD. The most significant limiting factor on the parameter determination was the low SNR of some spectra, while the spectral coverage and crowding in dense fields played less significant roles. We found that the metallicity is not consistent among the cluster members and it is still unclear what causes it. If the inconsistency is real a possible explanation would be the presence of multiple stellar populations within the cluster as mentioned by Geisler *et al.* (2012). To confirm this hypothesis a uniform spectroscopic survey is required.

MIST isochrones were fit to our CMD comprised of cluster members, including our variable star population. From our best three fits, we derived a metallicity range of 0.26 to 0.28 and the age of NGC 6791 to be 8.91 Gyr. Our age estimate agrees with the values reported by e.g. Choi *et al.* 2018. The average distance estimate from the distance modulus is 4134 pc which overlaps with our independent estimate of 4123(31) pc we derived from the *Gaia* astrometry.

## Acknowledgement

Financial support from the National Science Centre under projects No. UMO-2017/26/E/ST9/00703 and UMO-2017/25/B/ST9/02218 is acknowledged. PN acknowledges support from the Grant Agency of the Czech Republic (GAČR 22-34467S). The Astronomical Institute in Ondřejov is supported by the project RVO:67985815. This paper includes data collected



by the Kepler mission and obtained from the MAST data archive at the Space Telescope Science Institute (STScI). Funding for the Kepler mission is provided by the NASA Science Mission Directorate. STScI is operated by the Association of Universities for Research in Astronomy, Inc., under NASA contract NAS 5-26555. This work has made use of data from the European Space Agency (ESA) mission. *Gaia* (<https://www.cosmos.esa.int/gaia>), processed by the *Gaia* Data Processing and Analysis Consortium (<https://www.cosmos.esa.int/web/gaia/dpac/consortium>). Funding for the DPAC has been provided by national institutions, in particular the institutions participating in the *Gaia* Multilateral Agreement. This research has made use of the NASA/IPAC Extragalactic Database (NED), which is operated by the Jet Propulsion Laboratory, California Institute of Technology, under contract with the National Aeronautics and Space Administration. This research has used the services of [www.Astroserver.org](http://www.Astroserver.org) under reference XZR329. We thank the anonymous referee for valuable comments, which have significantly improved the quality of the manuscript.

## References

- Ahn C. P. et al. 2014, ApJ, 211, 17
- Baade W. 1931, Astronomische Nachrichten, 243, 303
- Baran A. 2013, AcA, 63, 203
- Basu S. et al. 2011, ApJ, 729, L10
- Bedin L. R. et al. 2005, ApJ, 624, 45
- Blanton M. R. et al. 2017, AJ, 154, 28
- Bohlin, R. C. M, é, sz, á, ros, S., Fleming, S. W. et al. 2017, AJ, 153, 234
- Borucki W. J. et al. 2010, Science, 327, 977
- Bressan A. M. et al. 2012, MNRAS, 427, 127-145
- Bryson S. T. et al. 2010, ApJ, 713, 97
- Bruntt H., Grundahl F., Tingley B., Frandsen S., Stetson P. B., Thomsen B. 2003, A&A, 410, 323
- Caldwell D. A. et al. 2010, ApJ, 713, 92
- Cardelli J. A. et al. 1989, ApJ, 345, 245
- Carraro G., Villanova S., Demarque P., McSwain M. V. and Piotto G., Bedin L. R., 2006, AJ, 643, 1151
- Carrera R. et al. 2019, A&A, 623, A80
- Chaboyer B., Green E. M., Liebert J. 1999, AJ, 117, 1360
- Chambers K. C. et al. 2016, arXiv, 1612, 05560
- Choi J., Dotter A., Conroy C., Cantiello M., Paxton B., Johnson B. D. et al. 2016, ApJ, 823, 102
- Choi J. et al. 2018, ApJ, 863, 65
- Colman I. L. et al. 2022, ApJS, 258, 39
- de Marchi F. et al. 2007, A&A, 471, 515
- Dempster A. P., Laird N. M., Rubin D. B. 1977, Journal of the Royal Statistical Society, 39, 1

Dotter A. 2016, ApJS, 222, 8

Fabricant D. et al. 2005, PASP, 117, 1411

Ferguson T. S. 1973, The Annals of Statistics, 1, 209

Flewelling H. A. et al. 2020, ApJ, 251, 7

*Gaia* Collaboration et al. 2016, A&A, 595, A1

*Gaia* Collaboration et al. 2021, A&A, 649, A1

Geisler D. et al. 2012, ApJ, 756, L40

Gilmore G. et al. 2012, The Messenger, 147, 25

Harris W. E. and Canerna R. 1981, AJ, 86, 1332

Hartman J. D., Stanek K. Z., Gaudi B. S., Holman M. J., McLeod B. A. 2005, AJ, 130, 2241

Howell S. B. et al. 2014, PASP, 126, 398

Jilkova L., Carraro G., Jungwiert B., Minchev I. 2012, A&A, 541, 64

Kaluzny J. and Rucinski S. M. 1993, MNRAS, 265, 34

Kaluzny J. and Udalski A. 1992, Acta Astronomica, 42, 29

Kaluzny J. 2003, Acta Astron., 53, 51

Kamann S., Bastian N. J., Gieles M., Balbinot E., Henault-Brunet V. 2019, MNRAS, 483, 2197-2206

Kinemuchi K. et al. 2012, Publications of the Astronomical Society of the Pacific, 124, 963

King I. R. 1964, Royal Greenwich Observatory Bulletins, 82, 106

Kinman T. D. 1965, ApJ, 142, 655

Koch D. G. et al. 2010, ApJ, 713, 79

Kwee K. and van Woerden H. 1956, Astronomical Institutes of the Netherlands, 12, 327

Liebert J., Saffer R. A., Green E. M. 1994, AJ, 107, 4

Lindgren L. et al. 2021, A&A, 649, A4

Majewski S. R. et al. 2017, AJ, 154, 94

Mochejska B. J. et al. 2005, AJ, 129, 2856

Mochejska B. J., Stanek K. Z., Kaluzny J. 2003, AJ, 125, 3175

Mochejska B. J., Stanek K. Z., Sasselov D. D., Szentgyorgyi A. H. 2002, AJ, 123, 3460

Né, meth, P., Kawka, A., Vennes, S. 2012, MNRAS, 427, 2180

Pedregosa F. et al. 2011, Journal of Machine Learning Research, 12, 2825

Platais I. et al. 2011, AJ, 733, 1

Randich S. et al. 2013, The Messenger, 154, 47

Rucinski S. M., Kaluzny J., Hilditch R. W. 1996, MNRAS, 282, 705

Sanjayan S. et al. 2022, MNRAS, 509, 763-777

Stetson P. B., Bruntt H., Grundahl F. 2003, PASP, 115, 413

Thompson, S, Fraquelli, D., Van Cleve, J., and Caldwell, D. 2016, KDMC, 10008,006

Tofflemire B. M., Gosnell N. M., Mathieu R. D., Platais I. 2014, AJ, 148, 61  
Villanova S., Carraro G., Geisler D., Monaco L., Assmann P. 2018, ApJ, 867, 34  
Zhao G. et al. 2012, A&A, 12, 7  
Ahn C. P. et al. 2014, ApJ, 211, 17  
Baade W. 1931, Astronomische Nachrichten, 243, 303  
Baran A. 2013, AcA, 63, 203  
Basu S. et al. 2011, ApJ, 729, L10  
Bedin L. R. et al., 2005, ApJ, 624, 45  
Blanton M. R. et al., 2017, AJ, 154, 28